12 Phase transitions, materials and applications

A. Gazizulina, S. Huangfu, A. Schilling, S. Siegrist, Q. Wang, W. Wang and X. Zhang

in collaboration with: University of Bern (K. Krämer), Deutsches Zentrum für Luft- und Raumfahrt (Prof. Alexei Semenov), Paul-Scherrer Institut (Dr. Marisa Medarde), Paul-Scherrer Institut (Dr. Ekaterina Pomjakushina, Dr. Vladimir Pomjakushin), McMaster University (Dr. Hanna Dabkowska), Max Planck Institute for Chemical Physics and Solids, Dresden (Prof. Claudia Felser), Universidad del Pais Vasco (Prof. Evgeny Sherman), Academy of Sciences of Uzbekistan (Prof. Abdulla Rakhimov), Leibniz-Institut für Festkörper- und Werkstoffforschung (IFW) (Dr. Vladimir Kataev), Helmholtz Research Centre Dresden-Rossendorf (Dr. Tobias Förster), Radboud University Nijmegen (Dr. Laurens Peters), Universitetet i Stavanger (Prof. Diana Quintero Castro), Helmholtz Zentrum für Materialien und Energie HZB (Dr. Illya Glavatskyy), Laboratoire National des Champs Magnetiques Intenses (lmcmi) (Dr. Albin De Muer), Deutsches Zentrum für Luft- und Raumfahrt (Dr. Heinz Wilhelm Hübers), Karlsruhe Institut für Technologie (Dr. Konstantin Ilín), National Institute of Standards and Technology (Dr. Sae Woo Nam), University of Geneva (Dr. Jeremie Teyssier), Dresden High Magnetic Field Laboratory (Dr. Sergei Zherlitsyn)

12.1 Superconducting nanowire single photon detectors (SNSPDs)

12.1.1 Criteria for choosing materials for SNSPDs

For superconducting photon detectors, the amount of photon energy consumed in breaking Cooper pairs is one of the most essential factors determining their detection efficiency. The energy of the incident photon is dissipated mainly through electron electron and electron-phonon interactions. The more energy is transferred into the electron subsystem, the higher the detection efficiency that can be expected. The likelihood for energy absorption through electron-electron interaction is $p_{e-e} \propto 1/\tau_{e-e}$ with the electron-electron interaction time τ_{e-e}, while $p_{e-ph} \propto 1/\tau_{e-ph}$ describes the corresponding contributions due to the interaction with the phonon subsystem. We have proposed a detailed model, concluding that materials with a large τ_{e-ph}/τ_{e-e} ratio (i.e., $p_{e-e} >> p_{e-ph}$) ensure that the photon energy can be effectively transferred to the material, and a more effective detector can be fabricated [1].

In a real material, the temperature dependences of τ_{e-ph} and τ_{e-e} near the critical temperature T_c can be determined by the magneto-transport measurements. From the excess magneto-conductance, the inelastic scattering time τ_i, containing a combination of τ_{e-ph} and τ_{e-e}, can be obtained at different temperatures and fitted with contributions of a weak localization effect, the Aslamazov-Larkin and Maki-Thompson fluctuation mechanisms, and the contribution from the suppression of the electronic density of states due to the formation of short lifetime Cooper pairs, respectively. In Fig. 12.1 we show the result of such fits to the excess magneto-conductance measured on a 4 nm-thick WSi film at different temperatures.

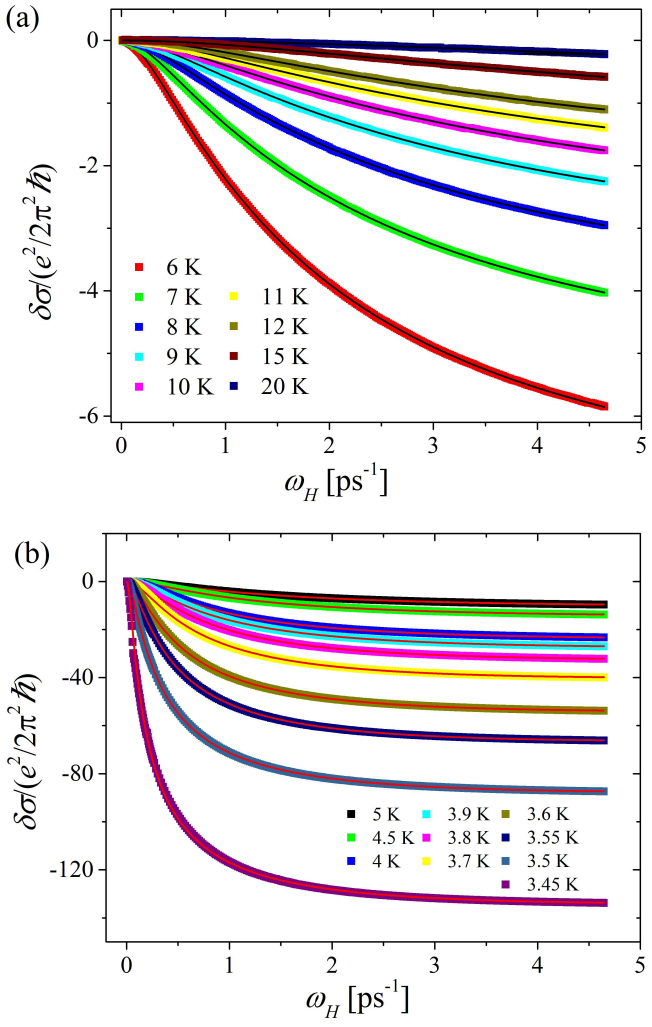

FIG. 12.1 – Best fits to the excess magneto-conductance of a 4 nm-thick WSi film at different temperatures.

The resulting temperature dependence of τ_i is shown in Fig. 12.2. From these data, we were able to extract the magnitudes and temperature dependences of τ_{e-e}, τ_{e-ph}, and a characteristic electron-fluctuation time τ_{e-fl} [1]. The temperature dependence of τ_{e-ph} follows αT^{-3} with $\alpha = 4.8\times10^3$ psK^3, which corresponds to τ_{e-ph} = 122 ps at the critical temperature (3.44 K) and 75 ps at 4 K. Sidorova et al. recently also studied the electron-phonon relaxation time in a 3.4 nm thick WSi film using an amplitude-modulated absorption of sub-THz radiation (AMAR) method, and τ_{e-ph} was estimated to be in the range of 100-200 ps at 3.4 K [2], which coincides well with our result from the magneto-resistance method. With respect to the contribution from the electron electron interaction, we obtain a temperature dependence $\tau_{e-e} = \beta T^{-1}$ with $\beta = 60$ psK, with $\tau_{e-e} = 17.4$ ps at T_c. Generally speaking, materials with a large τ_{e-ph}/τ_{e-e} ratio, such as WSi ($\tau_{e-ph}/\tau_{e-e} \approx 6.9$ for a 4 nm film at T_c) [1] or MoN ($\tau_{e-ph}/\tau_{e-e} \approx 11$ [3]), are more suitable for SNSPD applications as compared to conventional superconducting materials, such as NbN ($\tau_{e-ph}/\tau_{e-e} \approx 1$) [3].

[1] Zhang X., Lita A., Sidorova M., Q. Wang V., Verma and, Nam S., Semenov A., and Schilling A, *Superconducting fluctuations and characteristic time scales in amorphous wsi*, accepted in Phys. Rev. B, arXiv:1712.05019, 2017.

[2] Sidorova M., Semenov A., Korneev A., Chulkova G., Korneeva Yu., Mikhailov M., Devizenko A., Kozorezov A., and Goltsman G., *Electron-phonon relaxation time in ultrathin tungsten silicon film*, arXiv:1607.07321, 2016.

[3] Korneeva Y., Florya I., Vdovichev S., Moshkova M., Simonov N., Kaurova N., Korneev A., and Goltsman G., *Electron-phonon relaxation time in ultrathin tungsten silicon film*, IEEE Trans. Appl. Supercond., 27:2201504, 2017.

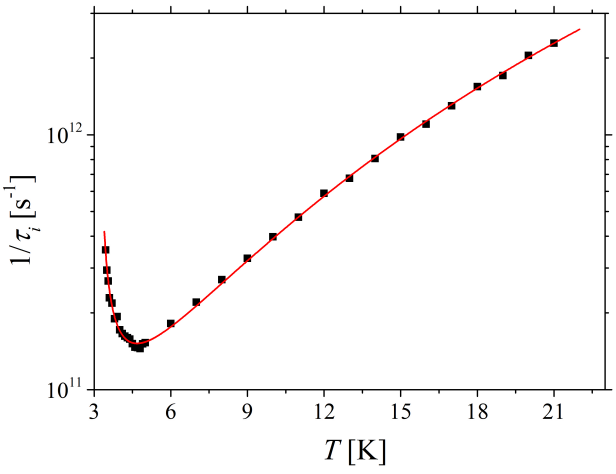

FIG. 12.2 – Measured inelastic scattering rate for a 4-nm thick WSi film.

12.1.2 X-ray single-photon detectors (X-SNSPDs)

Based on our previous experience with optical superconducting nanowire single-photon detectors (SNSPDs), we had extended their application range to the X-ray regime (see last annual reports and Refs. [4, 5]). These detectors had been structured from Nb, TaN and WSi superconducting films, and were successfully operating around liquid helium temperatures ($T \approx 4$ K).

In order to achieve a wider range of applicability, we are now attempting to adapt the same detection scheme to high-temperature superconductor films, with the potential to fabricate a detector operating at liquid nitrogen temperature (77 K). Although there are no reports on the successful implementation and operation of optical SNSPDs based on these materials in the literature, the preconditions for fabricating corresponding X-SNSPDs are more favorable. The reason is that SNSPDs for optical wavelengths require small dimensions of the superconducting wires, of the order of nanometers in width and thickness, which are difficult to produce and handle with ceramic high-temperature superconductors without significant degradation of their superconducting properties. By contrast, X-SNSPDs can (and should) be made from thick films to increase the absorption probability of X-ray photons, and the use of wide wires may also be feasible. We started with a simple bridge made of a commercial 150 nm thick $YBa_2Cu_3O_7$ film via electron beam lithography. Fig. 12.3 shows the SEM image of the 2.5 µm wide bridge with a critical temperature $T_c = 84$ K. Corresponding current-voltage I-V curves at $T = 72$ K and 76 K are shown in Fig. 12.4. The expected hysteretic behavior and the characteristic transition to the normal state at a well-

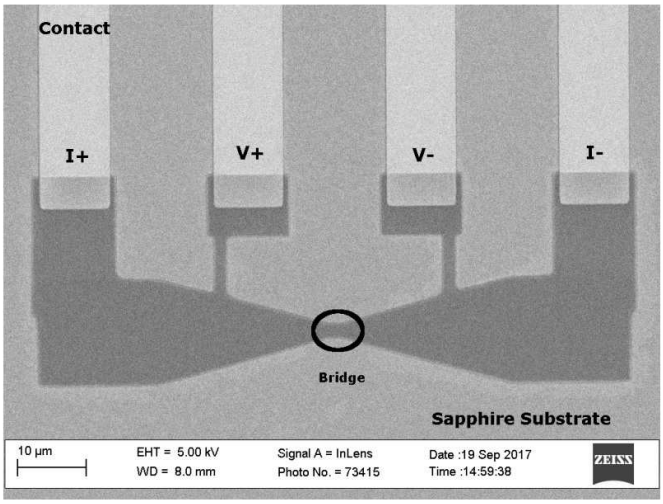

FIG. 12.3 – SEM image of the 2.5 µm wide $YBa_2Cu_3O_7$-bridge. The gold contacts for four-point measurements are indicated as (V+; V-; I+; I-).

defined critical current I_c are visible only at 72 K. The finite slope at small voltages is due to the circuit resistance. A well-defined I_c is crucial for the operation of the detector, because sharp detectable voltage pulses upon photon absorption are generated only if part of the current-biased superconductor becomes suddenly temporarily normal conducting.

For an X-ray detection measurement, we operated the $YBa_2Cu_3O_7$-bridge with 99 % of I_c at T = 72 K and irradiated it using an X-ray source with a W-target operating at 30 keV and 1.5 mA. After 20 min integration time, only 2 detection events were recorded. A detailed analysis showed that these detection events were most probably caused by thermal fluctuations in the bridge. As the $YBa_2Cu_3O_7$ film showed signs of degradation upon nano-fabrication, we are now working with 300 nm thick $(Bi, Pb)_2Sr_2Ca_2Cu_3O_{10}$ films with T_c = 108 K which are much more robust against oxygen loss as compared to $YBa_2Cu_3O_7$ films [6, 7] (in collaboration with A. Matsumoto, NIMS, Tsukuba, Japan).

[4] Inderbitzin K., Engel A., and Schilling A., *Soft x-ray single-photon detection with superconducting tantalum nitride and niobium nanowires*, IEEE Trans. Appl. Supercond., 23:2200505, 2013.

[5] Zhang X., Wang Q., and Schilling A., *Superconducting single x-ray photon detector based on $W_0.8Si_0.2$*, AIP Advances, 6:115104, 2016.

[6] Russek S., Sanders S., Roshko A., and Ekin J., *Surface degradation of superconducting $YBa_2Cu_3O_7$ thin films*, Appl. Phys. Lett., 64:3649, 1988.

[7] Maeda H., Tanaka Y., Fukutomi M., and Asano T., *Synthesis of BiSrCaCuo ceramics with large intergrowth defects*, Jpn. J. Appl. Phys., 27:209, 1994.

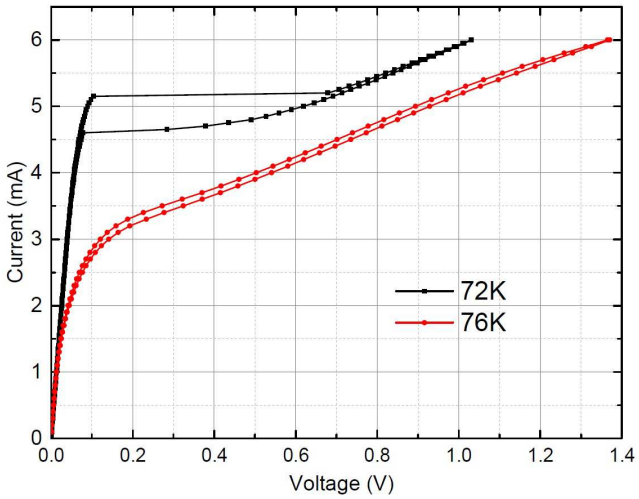

FIG. 12.4 – I-V curves of the $YBa_2Cu_3O_7$-bridge.

12.2 New results on the system $Ba_{3-x}Sr_xCr_2O_8$

The solid-solution $B_{3-x}Sr_xCr_2O_8$ was described in detail in the annual reports from previous years. To be short, these compounds are dimerized spin $\frac{1}{2}$ systems with a strong antiferromagnetic interaction that leads to a singlet ground state and energetically separated triplet states. This separation can be closed by a magnetic field (at a critical field H_{c1}) due to the Zeeman effect, thereby introducing antiferromagnetic order. This state resembles a Bose-Einstein condensate of magnetic quasiparticles, so called 'triplons'. In the past years we had studied the dependence of the magnetic interactions and the critical fields as functions of x by various techniques, and we showed that these quantities can be tuned between the extremal values in $Sr_3Cr_2O_8$ and $Ba_3Cr_2O_8$ [8,9].

Last year we have continued this line of research, e.g., by Raman spectroscopy measurements (in collaboration with Univ. of Geneva, Dr. J. Teyssier) on single crystals of $Ba_{0.2}Sr_{2.8}Cr_2O_8$ and $Ba_{0.1}Sr_{2.9}Cr_2O_8$, to study a high-temperature structural phase transition from hexagonal to monoclinic upon lowering the temperature.

To complete the magnetic phase diagram of $Ba_{0.1}Sr_{2.9}Cr_2O_8$ presented in Ref. [9], we have performed a series of ultrasound velocity measurements on single crystals of $Ba_{0.1}Sr_{2.9}Cr_2O_8$ at the Dresden High Magnetic Field Laboratory (in collaboration with Dr. S. Zherlitsyn) using a pulse-echo method with a phase-sensitive detection technique. The ultrasound frequencies ranged between 5 and 500 MHz, with magnetic field pulses up to almost 60 T during 120 ms. In Fig. 12.5(left) we show the relative changes of the sound velocity, exhibiting two distinct features around 30 T and 50 T, respectively. The corresponding magnetic phase diagram is shown in Fig. 12.5(right), together with respective data taken from the literature for $Sr_3Cr_2O_8$ (x = 3) [10].The nature of the phase labeled as 'magnonic liquid' in Fig. 12.5(right) and in Ref. [10] is still a matter of debate. While it is clear that it represents a state outside the antiferromagnetic 'dome' (here labeled as 'magnonic superfluid' [10]), little is known about its microscopic origin.

[8] Gazizulina A., Quintero-Castro D., and Schilling A., *Single-crystal growth and study of the mixed spin-dimer system $Ba_{3-x}Sr_xCr_2O_8$*, Physical Review B, 96:184201, 2017.

[9] Grundmann H., Gazizulina A., Schilling A., von Rohr F., Forster T., and Peters L., *Tuning the critical magnetic field of the triplon Bose-Einstein condensation in $Ba_{3-x}Sr_xCr_2O_8$*, New J. Phys., 18:033001, 2016.

[10] Wang Z., Quintero-Castro D., Zherlitsyn S., Yasin S., Skourski Y., and Loidl A., *Field-induced magnonic liquid in the 3d spin-dimerized antiferromagnet $Sr_3Cr_2O_8$*, Phys. Rev. Lett., 116:147201, 2016.

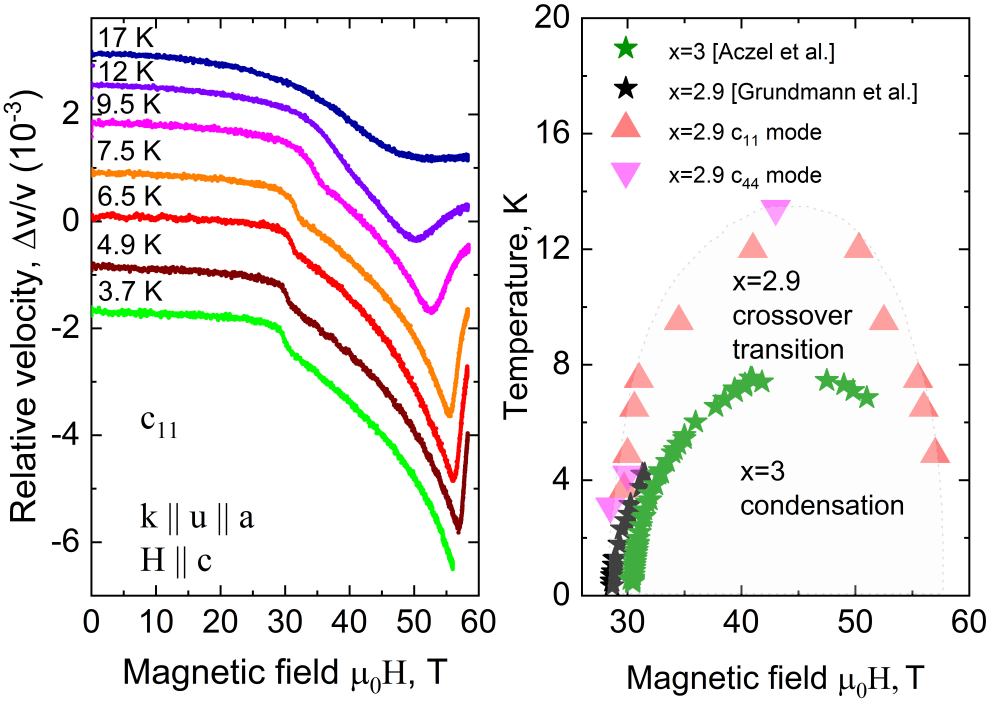

FIG. 12.5 – Left: changes in the sound velocity of a $Ba_{0.1}Sr_{2.9}Cr_2O_8$ single crystal in pulsed magnetic fields. Right: extracted magnetic phase diagram, together with data from our Ref. [9] and Ref. [10].

12.3 Investigations on $Pr_4Ni_3O_8$, a trilayer nickelate

The trilayer nickelates $La_4Ni_3O_8$ and $Pr_4Ni_3O_8$ (Fig. 12.6) show a large orbital polarization with unoccupied Ni *3d* states that are predominately $d_{(x^2-y^2)}$ in character, with a low spin configuration for dopants (Ni^{2+} holes), and a high degree of hybridization between Ni *3d* and O *2p* states [11]. This is very reminiscent of the situation met in the well-known superconducting copper oxides.

In their stoichiometric composition, the filling of the *3d* states corresponds, in the language of the cuprates, to a state which is highly overdoped with holes. Most interestingly, $Pr_4Ni_3O_8$ has indeed been reported to be metallic [11], while $La_4Ni_3O_8$ is not. It is therefore natural to attempt to change the number of charge carriers in these compounds by doping, possibly up to the level of reaching an antiferromagnetic insulating phase, which would then be an analogue to the 'parent structure' of the cuprates [12], and to examine their physical properties.

In Fig. 12.7 we show a series of magnetic hysteresis loops of $Pr_4Ni_3O_8$, suggesting that the compound is, in fact, ferro- or ferrimagnetic. We have also studied the preparation conditions and possibilities to change the cation and anion stoichiometry of $Pr_4Ni_3O_8$. While cation substitution by atoms of different valency (e.g., by partially replacing Pr^{3+} with Ce^{4+}) was not successful, we succeeded in varying the oxygen content to a large extent

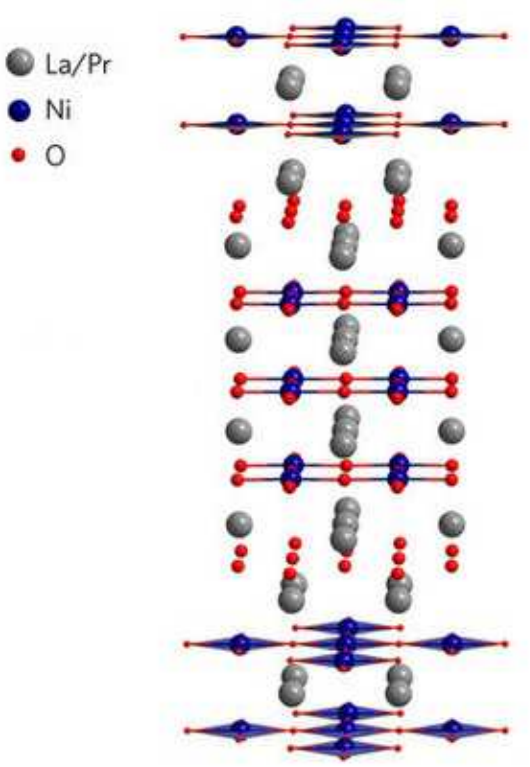

FIG. 12.6 – Crystal structure of the trilayer nickelates $La_4Ni_3O_8$ and $Pr_4Ni_3O_8$ (taken from Ref. [11]).

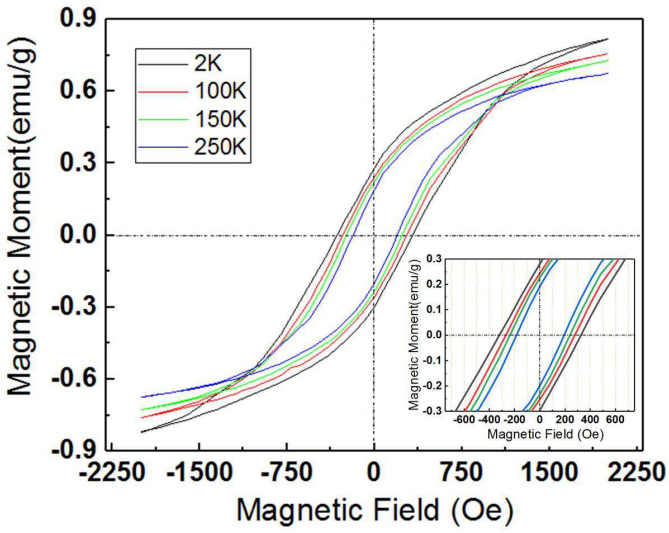

FIG. 12.7 – Magnetic hysteresis loops of $Pr_4Ni_3O_8$ measured at 2K, 100K, 150K and 250K.

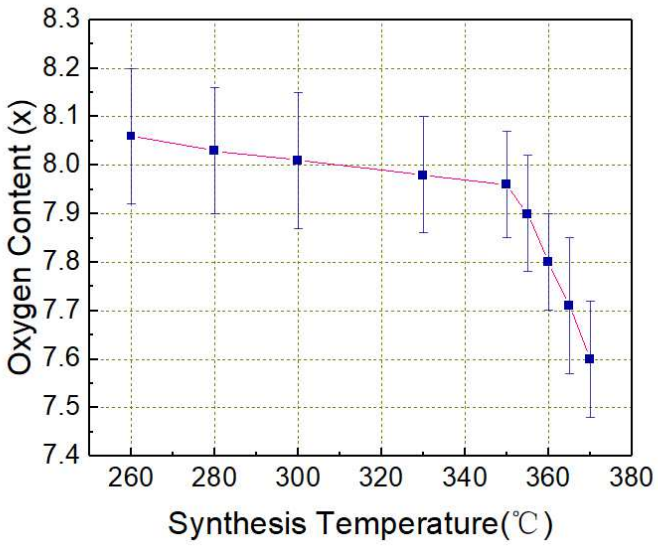

FIG. 12.8 – : Oxygen content of $Pr_4Ni_3O_8$ as a function of synthesizing temperature.

by adjusting the synthesizing temperature of $Pr_4Ni_3O_8$ in a mixture of N_2/H_2 while maintaining the crystal structure intact. In Fig. 12.8, we show the dependence of the oxygen content which we determined by titration techniques, on the respective synthesizing temperature.

Based on these investigations, we plan to perform a neutron-scattering study (in collaboration with V. Pomjakushin, PSI Villigen), to investigate the details of the oxygen sublattice in oxygen-deficient $Pr_4Ni_3O_8$.

[11] Zhang J., Botana A., Freeland J., Phelan D., Zheng H., Pardo V., Norman M., and Mitchell J., *Large orbital polarization in a metallic square-planar nickelate*, Nature Physics, 13:864, 2017.

[12] Botana A., Pardo V., and Norman M., *Electron doped layered nickelates: Spanning the phase diagram of the cuprates*, Physical Review Materials, 1:021801, 2017.